Green Fabrication of Silica with Zinc Oxide as Nanocomposite for Adsorption of Methylene Blue Dye from Aqueous Solution

Shahad Luay Maatoq and Inaam Hussein Ali*

Department of Chemistry, College of Science for Women, University of Baghdad, Baghdad 10071, Iraq

* Corresponding author:

email:

inaamha_chem@csw.uobaghdad.edu.iq

Received: February 14, 2025 Accepted: June 29, 2025

DOI: 10.22146/ijc.104761

Abstract: A nanocomposite of silica and zinc oxide was synthesized by a green route approach by utilizing aspartic acid as a reduction agent of Zn^{+2} in the precursor $ZnSO_4$ - $7H_2O$. Different methods like FTIR, BET surface analysis, SEM, and XRD characterized the resulted Zn-Si NC. The adsorption efficiency of the sample was examined by adjusting some variables to remove methylene blue dye from an aqueous solution. The data were analyzed using different models for studying the behavior of the synthesized sample. The Freundlich model is a better predictor than the Langmuir model with a high R^2 . Also, Temkin and Dubinin-Radushkevich (D-R) isotherms were applied and reveal that the adsorption energy calculated using the D-R isotherm was less than $8 \, kJ \, mol^{-1}$, indicating that the behavior of the process was physisorption. The kinetic data matched exactly with the pseudo-first-order model. The adsorption process is spontaneous due to a negative value of ΔG and exothermic, as the value of ΔH was $-9.616 \, kJ \, mol^{-1}$. The Si-Zn nanocomposite was successfully biosynthesized as a clean adsorbent to remove MB dye from wastewater.

Keywords: aspartic acid; silica; zinc oxide; nanocomposite; methylene blue

■ INTRODUCTION

Contamination of water has been considered one of humanity's largest fears. Many pollutants can negatively affect the water resource, including heavy metals, antibiotics, pesticides, polycyclic aromatic hydrocarbons and dyes [1]. Methylene blue (MB) is one of the most widely used dyes for coloring materials in many industries such as textiles, papers, plastics, cosmetics, and foods. [2]. It is a highly soluble cationic dye in water due to its positive charge. Low dosages of methylene blue are harmless, but high levels can have negative effects, such as excessive hemoglobin and digestive disorders. Because of the possibility of drug interactions, it should only be administered under medical guidance [3]. To deal with this challenge, numerous technologies have been developed to clean wastewater, including reverse osmosis [4], chemical precipitation [5], membrane filtering [6], and photodegradation [7]. However, there are limitations to these treatments, such as high implementation and operation costs, weak removal effectiveness, and harmful residues [8]. Researchers have placed a lot of emphasis on

the adsorption procedure since it is certainly one of the most successful techniques for eliminating contaminants from wastewater. In this instance, nanoparticles (NPs) have garnered a lot of interest due to their distinct qualities in contrast to bulk material [9]. Many advantages are associated with metal oxide NPs and silica-metal oxide nanocomposites, including high surface area, low concentration, easy separation after administration, and more [10].

Chemical and physical procedures represent the main routes for the synthesis of NPs using metal and metal oxide [11]. Precipitation [12], the sol-gel technique [13], and chemical reduction [14] are the most studied chemical synthesis methods, whereas indications of microwave-assisted combustion [15], laser evaporation [16], and pulsed laser deposition [17] were found in the physical synthesis routes. However, these techniques have several drawbacks, such as the use of hazardous materials, inefficiency in terms of cost, risky practices, and the creation of hazardous byproducts that are bad for the environment [18].

Doping can also be used to improve the properties and surface area of metal NPs. Of all the coating materials, silica is certainly the most well-researched and widely utilized [19]. Besides making NPs more stable in aqueous solutions, silica provides a framework that may be customized to accommodate different functional groups. The green route, which employs materials with minimal or no toxicity, is the most promising method for producing metallic NPs. There are certainly multiple applications for the developed metallic NPs in medicine, agriculture, food, sensors, optics, biomedical sciences, drug delivery, cosmetics, light emitters, electronics, and water purification [20]. Additionally, materials based on nano-silica offer a non-toxic and environmentally acceptable adsorbent. Numerous researchers have looked into various silica-based NPs for the removal of dyes from wastewater. As an efficient adsorbent for the removal of crystal violet, Hasan et al. [21] reported the production of mesoporous silica NPs covered by a copolymer chain of L-ascorbic acid and polyaniline. Their results gave a maximal adsorption capacity of 88 mg g⁻¹ at 298 K, and the Langmuir model was able to fit the experimental results. In another study, Alswieleh [22], investigated modifying mesoporous silica NPs with L-arginine to remove ionic dyes from aqueous solution and revealed that adsorption experiments were affected by different operation parameters.

Aspartic acid, an a-amino acid, is utilized in the formation of proteins, whereas L-aspartate is a glycogenic amino acid that can help increase energy generation through its Krebs cycle metabolism [23]. The use of α amino acids as capping and reducing agents in the synthesis of metal NPs has, however, been the subject of very few studies. In the previous work, functionalized AuNPs were synthesized using aspartic acid, which functions as a reductant and stabilizer, without the need for any further surface modification steps, where the product has the same good stability and optical characteristics as citrate-stabilized AuNPs [24]. By searching the previous works, no researchers were found who used aspartic acid as a reduction agent in the synthesis of modified silica NPs. This study aims to develop a process that uses silica as a matrix and aspartic acid as a green reduction component to enhance silicazinc oxide nanoparticles' size, shape, and chemical and physical properties. Various spectroscopic methods, including BET SEM, FTIR, XRD, and others, can be used to characterize the prepared nanocomposite. The obtained nanocomposite will then be employed in an adsorption method to remove MB dye from an aqueous solution.

EXPERIMENTAL SECTION

Materials

Two precursors used in the synthesis procedure, namely tetraethoxysilane (TEOS) as a silica source and zinc sulphate ($ZnSO_4$ · $7H_2O$) as a zinc source, were purchased from Sigma-Aldrich. Aspartic acid was purchased from BDH.

Instrumentation

UV-visible (UV-1800, Shimadzu) and FTIR (Prestige 21 Fourier Transform, Shimadzu) analyses were provided by University of Baghdad, Iraq. BET surface area (Micrometric ASAP2020 V3.04), scanning electron microscope (SEM, Oxford instruments model 3200N), and X-ray diffraction (XRD, Siemens model D500) measurements were done in University of Kashan, Iran.

Procedure

The synthesis method of Si-Zn oxide NC was carried out by mixing 10 mL of aqueous solution of 1 M ZnSO₄ with 10 mL of 1 M TEOS. The mixture was vigorously stirred for 3 h while 50 mL of 0.5 M aspartic acid was added dropwise. Then 25 mL of 1% starch was added gradually, and an aqueous solution of NaOH was slowly added to the mixture to adjust the pH to 8 to obtain an off-white precipitate. After filtering, the resulting precipitate was thoroughly washed with deionized water. The precipitate was dried for 24 h overnight, then in an oven at 100 °C, and crushed to fine powder using agate mortar for characterization.

The efficiency of the synthesized Si-Zn NC as an adsorbent was examined to remove MB dye from aqueous solution using batch experiments. A specific amount of Si-Zn oxide NC was added to 50 mL of dye.

The dye solution's initial concentration was 10 mg L^{-1} . A thermostatic shaker (Julabo SW23) was used to shake the mixture. The parameters evaluated in the batch studies were dye initial concentration (4–18 mg L^{-1}), adsorbent dosage (0.05–0.25 g), and contact time (10–80 min). To remove the adsorbent from the aqueous solution, a sample (2 mL) of each solution is taken out of each flask and filtered using a centrifuge (R8C, REMI centrifuge, India). To determine the amount of dye that remained in the filtered solution, a double beam UV-visible spectrophotometer (Shimadzu (China) Co., Ltd.) was used at $\lambda_{max} = 556$ nm. The quantity of the MB dye adsorbed by the Si-Zn NC has been determined using Eq. (1) [25]:

$$q_e = \frac{\left(C_0 - C_e\right)V}{W} \tag{1}$$

where q_e is the quantity of the MB adsorbed to the weight of Si-Zn NC; C_0 is the initial MB concentration and C_e is the concentration of the dye after attaining the equilibrium; V is the volume of the sample; and w is the quantity of the adsorbent Si-Zn NC added.

RESULTS AND DISCUSSION

Characterization

FTIR

The green reduction material's functional groups that support the bonding mechanism with SiO_2 and ZnO NPs were identified using FTIR analysis. The FTIR spectra of the Si-Zn NC (Fig. 1) show a characteristic peak

of the Zn–O bonding at 617 cm⁻¹. It is reasonable to propose that the extract's functional groups provide electrons that could reduce zinc ions (Zn²⁺ to Zn⁺) and, eventually, zinc nanoparticles (Zn⁰) [26]. Strong and broad peaks are also apparent, reflecting the complicated structure of the stretching of the O–H bond, which is represented by the sharp peak with high absorption intensity at 3410 cm⁻¹. Also, the biosynthesized Si-Zn NC's FTIR spectrum revealed a prominent spectral area (with respect to Si) at 1115 cm⁻¹, with accompanying shoulders that are assigned to asymmetric stretching vibrations of Si–O–Si [27].

XRD

Fig. 1(b) shows the synthesized XRD patterns for the Si-Zn NC. The strong diffraction peaks of the produced nanocomposite reflect its good crystallinity. Particularly (100), (002), and (101), the strong and narrow diffraction peaks demonstrated an excellent crystal structure and high-quality peak intensities. The diffraction peaks in the XRD pattern revealed the hexagonal crystal structure of Si-Zn NC [28]. The nanocrystallites' estimated sizes were between 7 and 25 nm. High extremely peaks of about 2θ at the numbers 32.5° , 34.5° , 36.4° , and 47.6° , corresponded to the planes of (100), (002), (101), and (102), orientations, respectively.

BET surface analysis

BET analysis, employing physical gas adsorption of nitrogen at 77 K, is an optimal method for measuring and

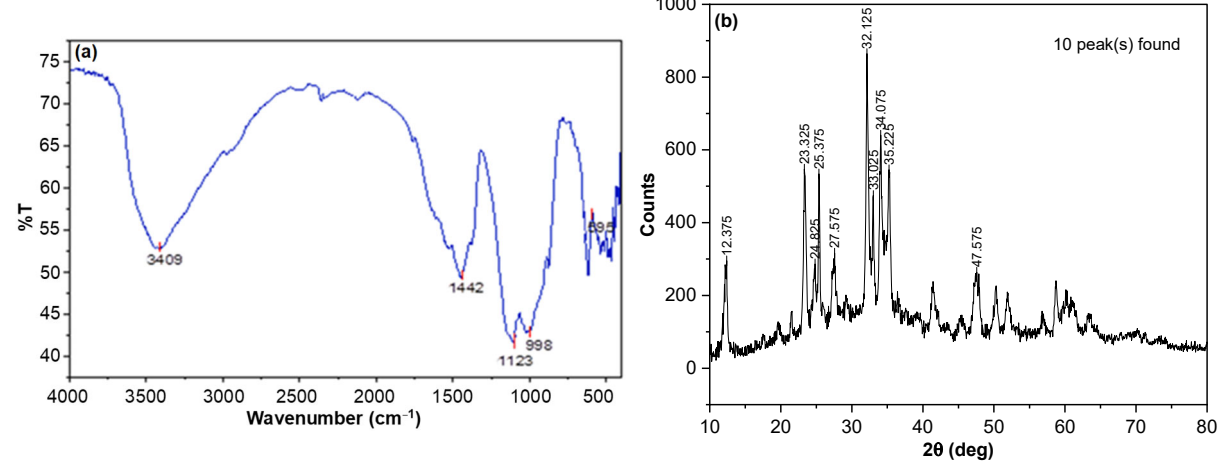


Fig 1. (a) FTIR spectra and (b) XRD pattern for the biosynthesized Si-Zn NC

quantifying the specific surface area of nanoparticle materials. Fig. 2 shows the adsorption-desorption isotherm of the synthesized Si-Zn NC. The obtained isotherm is a typical type–IV isotherm and has H1 type hysteresis loop, which indicates the formation of cylindrical pores [29]. The values measured for BET surface area, Barrett-Joyner-Halenda (BJH) pore diameter, and pore volume were 10.424 m² g⁻¹, 14.02 nm, and 3.35 cm³ g⁻¹ respectively.

SEM

This technique was performed for the aim of determining surface morphology, size, and three-dimensional photographs of NPs [30]. Fig. 3 illustrates the agglomerated form of Si-Zn NC with various magnifications, which is evident that the tiny particles are stacked in different sizes, creating a multi-layered array. The image reveals a number of rough, uneven, and irregularly shaped pores. Higher contact areas and easy pore diffusion during the adsorption process are characteristics of these pores. There were also many cage-

like cavities, which were particularly effective at removing dye because they had more locations for the reaction to occur due to the porosity and number of cavities.

Adsorption Behavior of Methylene Blue on Si-Zn Oxides Composite

Effect of Si-Zn oxides NC dosage

Different dosages of Si-Zn oxide nanocomposite were taken (0.05, 0.10, 0.15, 0.20, 0.25 g) to examine which is the best to evaluate a higher adsorbed quantity of MB dye. Each of these doses was added to 50 mL of 10 mg L⁻¹ of MB dye at 25 °C. Fig. 4(a) shows that dye uptake at equilibrium (q_e) decreases as the dosage of Si-Zn nanocomposite increases and the maximum amount of MB dye adsorbed was reached when 0.05 g of Si-Zn nanocomposite, so this dosage was used in all remaining experiments. This is mainly because there is less of a driving force between the concentration of the MB dye in the solution and the particle surface of the Si-Zn nanocomposite [31]. As a result, there is less competition

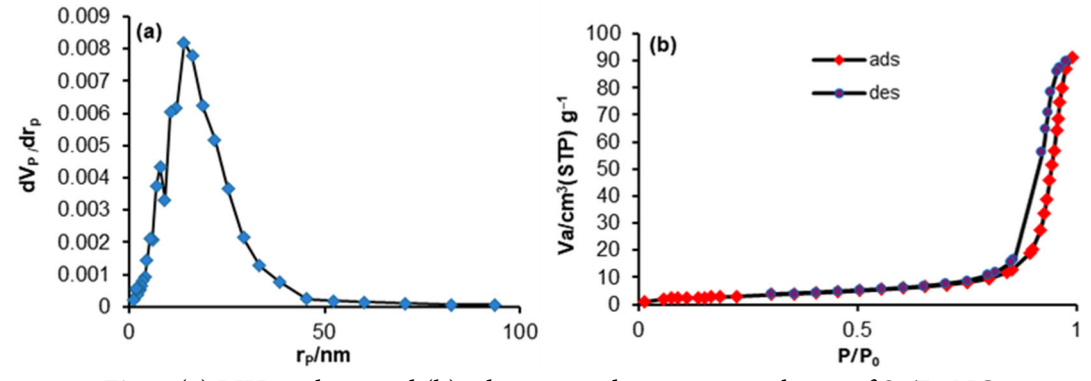


Fig 2. (a) BJH analysis and (b) adsorption-desorption isotherm of Si-Zn NC

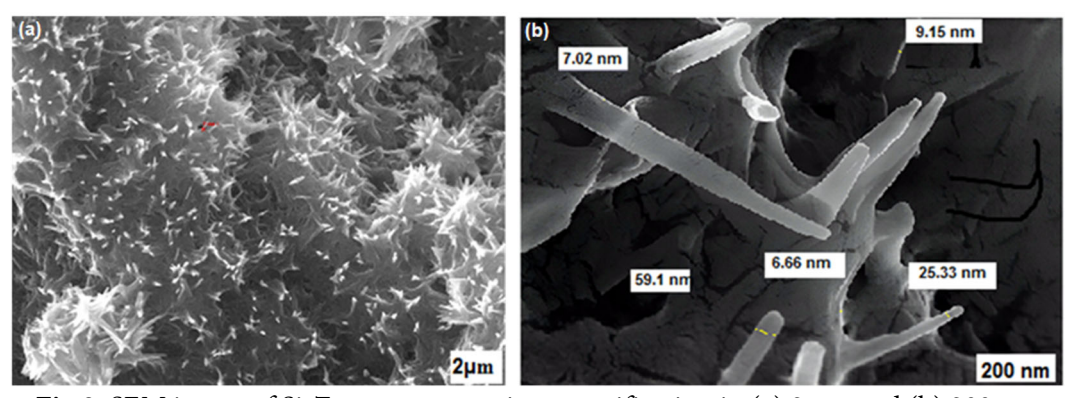


Fig 3. SEM image of Si-Zn nanocomposite, magnification in (a) 2 μm and (b) 200 nm

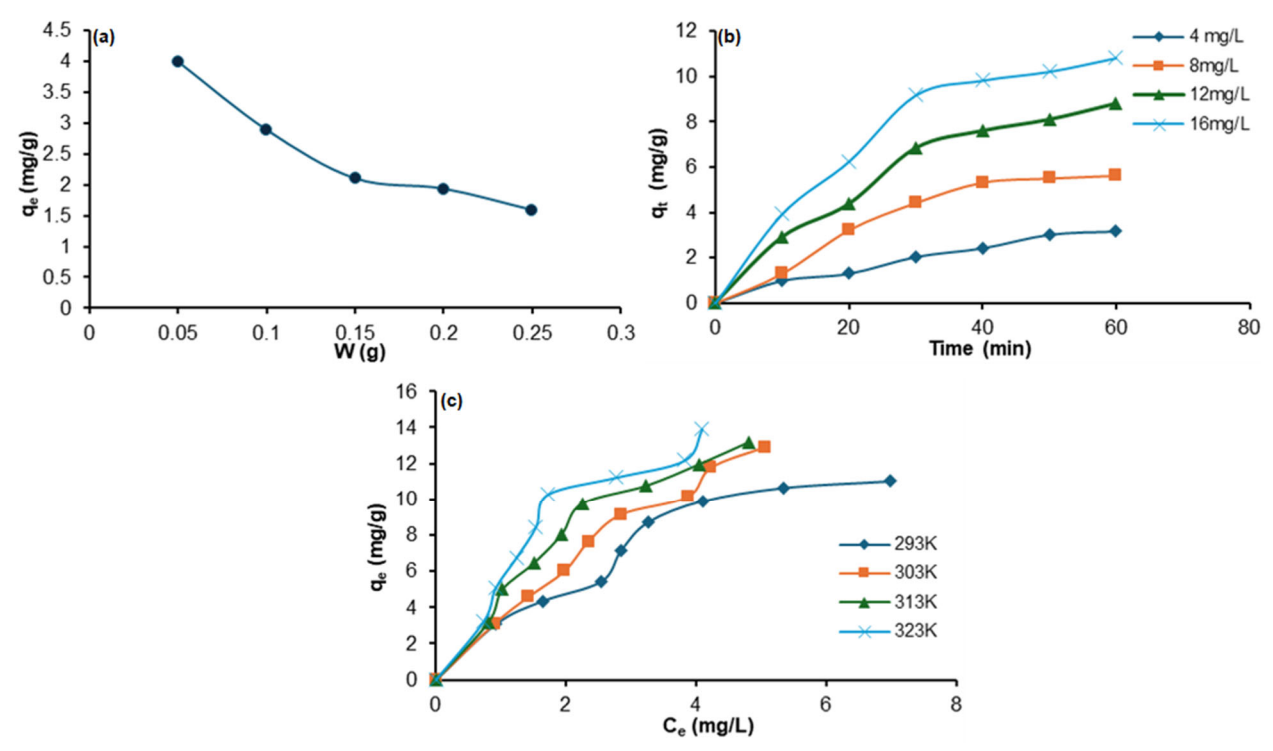


Fig 4. Adsorption of MB with variation of (a) Si-Zn NC doses, (b) time and concentration, and (c) initial concentration and temperature

for the available binding sites for MB dye adsorption as the dosage of the Si-Zn nanocomposite increases.

Effect of MB dye initial concentration

Fig. 4(b) illustrates the evaluation of the influence of contact time on MB dye adsorption at varied time intervals and different dye concentrations. The adsorption process was seen to be rapid during the initial contact period and then slowed down after that. It took 60 min to reach the equilibrium for MB adsorption on the Si-Zn NC surface. This could be because there are initially a lot of adsorption sites available, but as time goes on, the number of adsorption sites decreases [32].

Adsorption Isotherm of MB on Si-Zn Oxides Composite

Adsorption isotherms can be employed to investigate the relationship between the amounts of dye adsorbed on the adsorbent at equilibrium. Fig. 4(c) illustrates the relationship between the quantity of MB adsorbed and its concentration at equilibrium at four temperatures. These curves start off with a slight slope and then rise sharply, showing that the curve is an S-shape

curve in accordance with Giles' categorization [33]. These isotherms show that the surface's affinity for the adsorptive is low at low concentrations and increases at higher concentrations.

The Langmuir, Freundlich, Temkin, and Dubinin-Radushkevich (D-R) isotherm equations were fitted to the adsorption data to compare the equilibrium results. A monolayer of homogeneous, adsorbing molecules is assumed to not interact, and a constrained site is assumed by Langmuir's adsorption isotherm, which is represented in Eq. (2) [34];

$$\frac{C_{e}}{q_{e}} = \frac{1}{K_{L}q_{0}} + \frac{C_{e}}{q_{0}} \tag{2}$$

where K_L is the energy adsorption constant, and q_0 is the maximum adsorption capacity. q_0 and K_L were calculated using the slope and intercept of a linear plot of C_e/q_e versus C_e . The application of the Langmuir isotherm equation to MB dye adsorption is shown in Fig. S1(a).

Freundlich isotherm [35], this model assumes a heterogeneous surface with adsorption capacity and is based on the Langmuir isotherm (Eq. 3);

$$\ln q_e = \ln K_f + \frac{1}{n} \ln C_e \tag{3}$$

where K_f is the Freundlich constant, which represents the adsorption capacity, while the dimensionless constant n is associated with the efficiency of adsorption. The value of n indicates the degree of nonlinearity between the dye concentration and the adsorption process. The intercept and slope of the fitted line of $\ln q_e$ against $\ln C_e$, as shown in Fig. S1(b), were used to get the values of K_f and n, respectively.

A parameter in the Temkin isotherm adequately accommodates interactions between the adsorbent and the adsorbate. By ignoring low and high concentration values, this model predicts that adsorption heat will decrease linearly with coverage instead of logarithmically. Plotting adsorbed q_e versus ln C_e yields the constants. As a result, binding is distributed uniformly throughout the derivation of Eq. (4). The following is a linear equation that represents the Temkin model [36];

$$q_e = B \ln K_T + B \ln C_e \tag{4}$$

where B = RT/b, where b is in joules per mole; R is the gas constant in joules; and K_T is the equilibrium binding constant of the Timken isotherm. The slope (B) and intercept (B ln K_T) of the q_e versus ln C_e plot can be used to figure out B and KT, as illustrated in Fig. S1(c).

In this work, D–R is another isotherm expression. The D-R isotherm for solid-liquid interaction has the following linear form (Eq. 5) [37].

$$lnq_e = lnq_m - \beta \varepsilon^2$$
(5)

Here (ε) is the Polanyi probability which equals;

$$\varepsilon = RT \ln \left(1 + \frac{1}{C_0} \right) \tag{6}$$

where β is a constant associated with adsorption energy (mol² Kj⁻²), q_m is a measure of the adsorbent's capacity, The D-R model can be used to predict the type of adsorption process by determining the mean adsorption energy ϵ .

$$E = \frac{1}{\sqrt{2\beta}} \tag{7}$$

Fig. S1(d) displays an application for the D-R model, and Table 1 shows the values of q_m , E, and R^2 for this model at four different temperatures.

When comparing the results shown in Table 1, and based on the values of R^2 , we find that the Freundlich model was more consistent with the results than the Langmuir model. The n values from the Freundlich model greater than unity showed a heterogeneous character of the adsorption and a positive cooperative interaction [38]. Additionally, the Langmuir equation's estimate of the maximal monolayer capacity (q_0) increased as the temperature increased, suggesting that the adsorption capacity increased at high temperatures.

The Temkin equation is useful for predicting equilibrium in the gas phase, but it is often not appropriate to represent the liquid-phase adsorption isotherms. Values for the b parameter in the Temkin model show performance that is distinct from what was observed for q_0 and q_s . Because there are more exposed adsorption sites in this temperature range (293–323 K), the interaction between the MB dye and Si-Zn NC

Table 1. Parameters	of MR adsorpt	ion isotherm m	odels onto Si-7r	NC
Table 1. Farameters	OF WID AUSOIDE	1011 18011161111 111	ひいという ひけけひ シローノオ	1 1 1 1 1 1

Models		Langmuir model				Freundlich model		
Temperature	\mathbb{R}^2	$q_0\ (mg\ g^{-1})$	K _L (L mg ⁻¹)		\mathbb{R}^2	$K_f (L mg^{-1})$	n	
293	0.8129	3.6680	5.8880		0.9435	3.2770	1.4350	
303	0.8298	3.7380	5.2400		0.9874	3.4850	1.1960	
313	0.8518	5.5130	4.9690		0.9423	4.5440	1.3660	
323	0.7317	6.8170	3.9860		0.8838	5.3430	1.3700	
Models		Temk	kin model			D-R mode	el	
Temperature	\mathbb{R}^2	В	$b_T (J \text{ mol}^{-1})$	$K_T (L g^{-1})$	\mathbb{R}^2	$q_m \ (mg \ g^{\scriptscriptstyle -1})$	E (kJ mol ⁻¹)	
293	0.9266	5.8440	386.3000	1.6240	0.9901	1.8620	3.1620	
303	0.9693	5.6160	420.6000	1.6470	0.9869	1.9410	3.5350	
313	0.9885	5.4380	467.2000	2.3190	0.9871	1.9740	3.5350	
323	0.9546	4.4890	588.9000	3.5420	0.9872	2.0110	3.5350	

adsorbent is probably stronger [39]. Adsorption energy (E) calculated using the D-R isotherm was less than 8 kJ mol⁻¹, indicating that physisorption clearly illustrated the binding behavior of the adsorption of MB dye onto Si-Zn NC.

Kinetics Study

Kinetic adsorption studies predict how the dyes will adsorb and their way to reach equilibrium. Furthermore, the adsorption mechanism estimate is crucial to examine MB using intra-particle diffusion, pseudo-first order, and pseudo-second order models.

The linear equation form of the pseudo-first-order kinetic model is as follows in Eq. (8) [40].

$$\log(q_e - q_t) = \log q_e - (k_1/2.303)t$$
 (8)

In the above equation, q_e and q_t are the amount of MB adsorbed on the surface at equilibrium and at any time, respectively, while k_1 is the rate constant of the pseudofirst order kinetics. When plotting log (q_e-q_t) versus.t, q_e and k_1 are frequently determined via the intercept and slope, respectively, as shown in Fig. S2(a).

Eq. (9) is the linear form of the pseudo-second order kinetic model [41];

$$\frac{t}{q_t} = \frac{1}{k_2 q_e^2} + \left(\frac{1}{q_e}\right)t\tag{9}$$

where k_2 is the rate constant for pseudo-second-order kinetics. As illustrated in Fig. S2(b), k_2 and q_e are calculated from the intercept and slope of plots of t/q_t against t, respectively.

The following equation represents how the Weber-Morris intra-particle distribution calculation is expressed in Eq. (10) [42];

$$q_t = k_i t^{0.5} + C (10)$$

where C is intercepted and k_i is the intra-particle diffusion rate constant. This model illustrates how the adsorbent's porousness contributes to pore diffusion. Being can calculate the rate constant of the intra-particle diffusion

 (k_i) by estimating the slope of the linear section of the plot of the quantity of solute adsorbed (q_t) against the square root of time $(t^{1/2})$ as shown in Fig. S2(c).

Table 2 indicates that the pseudo-first order equation's R² value is somewhat higher than the pseudo-second order kinetic model's R² value. This implies that the adsorption system's kinetics were more accurately modeled by the pseudo-first order kinetic model than by the pseudo-second order model. The slope was linear due to the intraparticle diffusion model, but the line did not pass through the origin, suggesting that intraparticle diffusion had a role in adsorption. But that wasn't the only rate-determining aspect, though; additional kinetic models may also be used to alter the adsorption rate [43].

Thermodynamic Parameters

Adsorption studies were conducted at four temperature ranges (293–323 K) to examine the thermodynamic functions, which are free energy change (ΔG°), enthalpy change (ΔH°), and entropy change (ΔS°) related to the interaction between MB dye and nanocomposite. The thermodynamic aspects have been obtained using Eq. (11) and (12) [44];

$$\Delta G^{\circ} = -RT \ln K_{I} \tag{11}$$

$$\ln K_{c} = \frac{\Delta S^{\circ}}{R} - \frac{\Delta H^{\circ}}{RT}$$
 (12)

where K_c is the equilibrium constant related to K_L . The slope and intercept of the van't Hoff plot of $\ln (K_c)$ against 1/T were used to estimate the values of enthalpy change and entropy change. This relationship is plotted in Fig. S3, and Table 3 displays the thermodynamic functions that were determined at four temperatures. The negative values of ΔG° confirm the feasibility and spontaneous adsorption nature. Since ΔH° was negative $(-9.616 \text{ kJ mol}^{-1})$, the adsorption reaction was exothermic. Additionally, in practice, ΔH° is less than 40 kJ mol^{-1} . This demonstrated that the mechanism of MB's adsorption onto Si-Zn NC was physisorption [45].

Table 2. Kinetics parameters of MB adsorption onto Si-Zn NC

			1		1			
Kinetics models	I	Pseudo-first-	order		Pseudo-second-or	der	Diffusion mo	del
Temperature (K)	\mathbb{R}^2	$k_1 \text{ (min}^{-1})$	$q_e (mg g^{-1})$	\mathbb{R}^2	$k_2(g\ mg^{-1}\ min^{-1})$	$q_e (mg g^{-1})$	$k_i (mg g min^{-0.5})$	\mathbb{R}^2
298	0.9851	0.0555	11.303	0.9474	0.0014	15.65	1.3386	0.964

	Temp. (K)	ΔG° (kJ mol ⁻¹)	ΔH° (kJ mol ⁻¹)	$\Delta S^{\circ} (J K^{-1} mol^{-1})$			
	392	-4.318					
	303	-6.095	0.616	-17.915			
	313	-4.172	-9.616	-17.913			
	323	-3.713					

Table 3. Thermodynamic parameters of MB adsorption onto Si-Zn NC

A decrease in adsorption capacity and a less irregular solid/liquid interface are the result of increasing temperature, that was indicated by negative value of ΔS° , which is -17.915 J K⁻¹ mol⁻¹.

CONCLUSION

Using aspartic acid as a reduction agent, Si-Zn nanocomposite was biosynthesized as a clean adsorbent to remove contaminants from wastewater. Various techniques, including FTIR, BET, SEM, and X-ray diffraction, were used to analyze the nanocomposite and ensure a successful doping process. In order to remove dye from aqueous solution, the synthesized sample's adsorptive performance was evaluated, and MB was selected as the toxic environmental dye. Fitting the adsorption parameters to various adsorption isotherms produced high agreement with the Freundlich isotherm and the thermodynamic investigation revealed excellent outcomes. Additionally, the experimental data closely match the pseudo-first-order kinetic model.

ACKNOWLEDGMENTS

Authors would like to express a deepest appreciation to Prof. Sameer H. Kareem for his valuable assistance and support that contributed to the work.

CONFLICT OF INTEREST

The authors declare no conflicts of interest.

AUTHOR CONTRIBUTIONS

Shahad Luay Maatoq gathering the experimental data and drafting the manuscript and Inaam Hussein Ali concepted the study, reviewed and revised the manuscript.

REFERENCES

[1] Salazar Sandoval, S., Bruna, T., Maldonado-Bravo, F., Jara, P., Caro, N., Rojas-Romo, C., González-

- Casanova, J., Gómez, D.R., Yutronic, N., Urzúa, M., and Rodríguez-San Pedro, A., 2023, Nanomaterials for potential detection and remediation: A review of their analytical and environmental applications, *Coatings*, 13 (12), 2085.
- [2] Nguyen, K.M., Pham, N.N., Tran, H.T.T., and Nguyen, S.T., 2025, Dual-functional Fe₃O₄@SiO₂/Ag/AgCl nanocomposites as photocatalyst for degrading methylene blue dye under natural light irradiation, *Indones. J. Chem.*, 25 (1), 169–177.
- [3] Khan, I., Saeed, K., Zekker, I., Zhang, B., Hendi, A.H., Ahmad, A., Ahmad, S., Zada, N., Ahmad, H., Shah, L.A., Shah, T., and Khan, I., 2022, Review on methylene blue: Its properties, uses, toxicity and photodegradation, *Water*, 14 (2), 242.
- [4] Liu, S., Sun, M., Wu, C., Zhu, K., Hu, H., Shan, M., Wang, M., Wu, K., Wu, J., Xie, Z., and Tang, H., 2024, Fabrication of loose nanofiltration membrane by crosslinking TEMPO-oxidized cellulose nanofibers for effective dye/salt separation, *Molecules*, 29 (10), 2246.
- [5] Hartal, O., Khattabi Rifi, S., Chatoui, M., Haddaji, C., Madinzi, A., Pala, A., and Souabi, S., 2024, Combined natural flotation and chemical precipitation for the treatment of vegetable oil refinery wastewater, *Int. J. Environ. Sci. Technol.*, 21 (10), 7295–7306.
- [6] Dehingia, B., Lahkar, R., and Kalita, H., 2024, Efficient removal of both cationic and anionic dyes from water using a single rGO/PSS nanocomposite membrane with superior permeability and high aqueous stability, *J. Environ. Chem. Eng.*, 12 (2), 112393
- [7] Shabil Sha, M., Anwar, H., Musthafa, F.N., Al-Lohedan, H., Alfarwati, S., Rajabathar, J.R., Khalid

- Alahmad, J., Cabibihan, J.J., Karnan, M., and Kumar Sadasivuni, K., 2024, Photocatalytic degradation of organic dyes using reduced graphene oxide (rGO), *Sci. Rep.*, 14 (1), 3608.
- [8] Kato, S., and Kansha, Y., 2024, Comprehensive review of industrial wastewater treatment techniques, *Environ. Sci. Pollut. Res.*, 31 (39), 51064–51097.
- [9] Alduhaidahawi, A.M.J., and Ahmed, A.A., 2024, Synthesis of TiO₂/ZnO nanocomposites by the electrochemical method and their application in dyesensitized solar cells (DSSCs), *Indones. J. Chem.*, 24 (1), 228–237.
- [10] Naseer, A., 2024, Role of nanocomposites and nano adsorbents for heavy metals removal and dyes. An overview, *Desalin. Water Treat.*, 320, 100662.
- [11] Nguyen, N.T.T., Nguyen, T.T.T., Nguyen, D.T.C., and Tran, T.V., 2023, Green synthesis of ZnFe₂O₄ nanoparticles using plant extracts and their applications: A review, *Sci. Total Environ.*, 872, 162212.
- [12] Baig, N., Kammakakam, I., and Falath, W., 2021, Nanomaterials: A review of synthesis methods, properties, recent progress, and challenges, *Mater. Adv.*, 2 (6), 1821–1871.
- [13] Patil, N., Bhaskar, R., Vyavhare V., Dhadge, R., Khaire, V., and Patil Y., 2021, Overview on methods of synthesis of nanoparticles, *Int. J. Curr. Pharm. Res.*, 13 (2), 11–16.
- [14] Hasan, S.H., and Alawadi, S.S.M., 2022, Reducing the purification period of Congo red dye solution by using co-exposure to ultraviolet and green laser as a photocatalyst source, *Iraqi J. Sci.*, 63 (5), 2025–2038.
- [15] Suresh Kumar, G., Srinivasan, R., Karunakaran, G., Kolesnikov, E., Kim, M., and Karpenkov, D.Y., 2021, Microwave-assisted combustion synthesis of soft ferromagnetic spinel MFe₂O₄ (M = Ni, Mg, Zn) nanoparticles using *Citrus limon* fruit extract as a fuel, *Appl. Phys. A*, 127 (7), 546.
- [16] Kim, M., Osone, S., Kim, T., Higashi, H., and Seto, T., 2017, Synthesis of nanoparticles by laser ablation: A review, *KONA Powder Part. J.*, 34, 80–90.

- [17] Shepelin, N.A., Tehrani, Z.P., Ohannessian, N., Schneider, C.W., Pergolesi, D., and Lippert, T.A., 2023, Practical guide to pulsed laser deposition, *Chem. Soc. Rev.*, 52 (7), 2294–2321.
- [18] Altammar, K.A., 2023, A review on nanoparticles: Characteristics, synthesis, applications, and challenges, *Front. Microbiol.*, 14, 1155622.
- [19] Nyabadza A., McCarthy, É., Makhesana, M., Heidarinassab, S., Plouze, A., Vazquez, M., and Brabazon, D., 2023, A review of physical, chemical and biological synthesis methods of bimetallic nanoparticles and applications in sensing, water treatment, biomedicine, catalysis and hydrogen storage, *Adv. Colloid Interface Sci.*, 321, 103010.
- [20] Joseph, T.M., Kar Mahapatra, D., Esmaeili, A., Piszczyk, Ł., Hasanin, M.S., Kattali, M., Haponiuk, J., and Thomas, S., 2023, Nanoparticles: Taking a unique position in medicine, *Nanomaterials*, 13 (3), 574.
- [21] Hasan, I., BinSharfan, I.I., Khan, R.A., and Alsalme, A., 2020, L-ascorbic acid-g-polyaniline mesoporous silica nanocomposite for efficient removal of crystal violet: A batch and fixed bed breakthrough studies, *Nanomaterials*, 10 (12), 2402.
- [22] Alswieleh, A.M., 2022, Efficient removal of dyes from aqueous solution by adsorption on Larginine-modified mesoporous silica nanoparticles, *Processes*, 10 (6), 1079.
- [23] Holeček, M., 2023, Aspartic acid in health and disease, *Nutrients*, 15 (18), 4023.
- [24] Figat, A.M., Bartosewicz, B., Liszewska, M., Budner, B., Norek, M., and Jankiewicz, B.J., 2023, α-Amino acids as reducing and capping agents in gold nanoparticles synthesis using the Turkevich method, *Langmuir*, 39 (25), 8646–8657.
- [25] Ali, I.H., 2021, Removal of Congo red dye from aqueous solution using eco-friendly adsorbent of nanosilica, *Baghdad Sci. J.*, 18 (2), 366–373.
- [26] Hussain, H.M., Mahmood, M.B., and Yaqoob, L.A., 2024, The biological effect of synthesized zinc oxide nanoparticles on organic pollutions in drinking water, *Iraqi J. Sci.*, 65 (8), 4246–4255.

- [27] Liu, H., Kaya, H., Lin, Y.T., Ogrinc, A., and Kim, S.H., 2022, Vibrational spectroscopy analysis of silica and silicate glass networks, *J. Am. Ceram. Soc.*, 105 (4), 2355–2384.
- [28] Manh, D.H., Ngoc Nha, T.T., Hong Phong, L.T., Nam, P.H., Thanh, T.D., and Phong, P.T., 2023, Determination of the crystalline size of hexagonal $La_{1-x}Sr_xMnO_3$ (x = 0.3) nanoparticles from X-ray diffraction a comparative study, *RSC Adv.*, 13 (36), 25007–25017.
- [29] Wang, Z., Jiang, X., Pan, M., and Shi, Y., 2020, Nanoscale pore structure and its multi-fractal characteristics of tight sandstone by N₂ adsorption/desorption analyses: A case study of Shihezi formation from the Sulige gas filed, Ordos Basin, China, *Minerals*, 10 (4), 377.
- [30] Al-darwesh, M.Y., Ibrahim, S.S., Faiad Naief, M., Mishaal Mohammed, A., and Chebbi, H., 2023, Synthesis and characterizations of zinc oxide nanoparticles and its ability to detect O₂ and NH₃ gases, *Results Chem.*, 6, 101064.
- [31] Sen, T.K., 2023, Adsorptive removal of dye (methylene blue) organic pollutant from water by pine tree leaf biomass adsorbent, *Processes*, 11 (7), 1877.
- [32] Rápó, E., and Tonk, S., 2021, Factors affecting synthetic dye adsorption; Desorption studies: A review of results from the last five years (2017-2021), *Molecules*, 26 (17), 5419.
- [33] Inglezakis, V.J., Poulopoulos, S.G., and Kazemian, H., 2018, Insights into the S-shaped sorption isotherms and their dimensionless forms, *Microporous Mesoporous Mater.*, 272, 166–176.
- [34] Sachit, M.A., and Kareem, S.H., 2023, Isotherms and thermodynamic parameters of metoprolol drug adsorption on the prepared mesoporous silica, *Baghdad Sci. J.*, 21 (3), 1029–1036.
- [35] Pereira, S.K., Kini, S., Prabhu, B., and Jeppu, G.P., 2023, A simplified modeling procedure for adsorption at varying pH conditions using the modified Langmuir–Freundlich isotherm, *Appl. Water Sci.*, 13 (1), 29.

- [36] Mabuza, M., Premlall, K., and Daramola, M.O., 2022, Modelling and thermodynamic properties of pure CO₂ and flue gas sorption data on South African coals using Langmuir, Freundlich, Temkin, and extended Langmuir isotherm models, *Int. J. Coal Sci. Technol.*, 9 (1), 45.
- [37] Batool, F., Kanwal, S., Kanwal, H., Noreen, S., Hodhod, M.S., Mustaqeem, M., Sharif, G., Naeem, H.K., Zahid, J., and Gaafar, A.R.Z, 2023, Ecofriendly synthesis of magnetic composites loaded on rice husks for Acid Blue 25 decontamination: Adsorption kinetics, thermodynamics, and isotherms, *Molecules*, 28 (20), 7124.
- [38] Kareem, S.H., Ali, I.H., and Jalhoom, M.G., 2014, Synthesis and characterization of organic functionalized mesoporous silica and evaluate their adsorptive behavior for removal of methylene blue from aqueous solution, *Am. J. Environ. Sci.*, 10 (1), 48–60.
- [39] Shah, S.S., Ramos, B., and Teixeira, A.C.S.C., 2022, Adsorptive removal of methylene blue dye using biodegradable superabsorbent hydrogel polymer composite incorporated with activated charcoal, *Water*, 14 (20), 3313.
- [40] Al-Harby, N.F., Albahly, E.F., and Mohamed, N.A., 2021, Kinetics, isotherm and thermodynamic studies for efficient adsorption of Congo red dye from aqueous solution onto novel cyanoguanidine-modified chitosan adsorbent, *Polymers*, 13 (24), 4446.
- [41] Kostoglou, M., and Karapantsios, T.D., 2022, Why is the linearized form of pseudo-second order adsorption kinetic model so successful in fitting batch adsorption experimental data?, *Colloids Interfaces*, 6 (4), 55.
- [42] Saad, E.M., Wagdy, M., and Orabi, A.S., 2024, Advanced nano modification of ecofriendly glauconite clay for high efficiency methylene blue dye adsorption, *Sci. Rep.*, 14 (1), 23614.
- [43] Wang, J., and Guo, X., 2023, Review on the intraparticle diffusion adsorption kinetics model:

- Interpretation, solving methods and applications, *Chemosphere*, 309 (Pt. 2), 136732.
- [44] Hiawi, F.A., and Ali, I.H., 2022, Study the adsorption behavior of food colorant dye indigo carmine and loratadine drug in aqueous solution, *Chem. Methodol.*, 6 (10), 720–730.
- [45] AL-Shehri, H.S., Alanazi, H.S., Shaykhayn, A.M., ALharbi, L.S., Alnafaei, W.S., Alorabi, A.Q., and Alkorbi, A.S., and Alharthi, F.A., 2022, Adsorption of methylene blue by biosorption on alkali-treated *Solanum incanum*: Isotherms, equilibrium and mechanism, *Sustainability*, 14 (5), 2644.